





Low-temperature pseudo-phase-transition in an extended Hubbard diamond chainOnofre Rojas  and S. M. de Souza*Departamento de Física, Universidade Federal de Lavras, 37200-900 Lavras, Minas Gerais, Brazil*Jordana Torrico *Departamento de Física, Universidade Federal de Minas Gerais, Caixa Postale 702, 30123-970 Belo Horizonte, Minas Gerais, Brazil*L. M. Veríssimo , M. S. S. Pereira, and M. L. Lyra *Instituto de Física, Universidade Federal de Alagoas, 57072-970 Maceió, Alagoas, Brazil*

(Received 1 December 2020; revised 18 February 2021; accepted 25 March 2021; published 14 April 2021)

We consider the extended Hubbard diamond chain with an arbitrary number of particles driven by chemical potential. The interaction between dimer diamond chain and nodal couplings is considered in the atomic limit (no hopping), whereas the dimer interaction includes the hopping term. We demonstrate that this model exhibits a pseudo-transition effect in the low-temperature regime. Here, we explore the pseudo-transition rigorously by analyzing several physical quantities. The internal energy and entropy depict sudden, although continuous, jumps which closely resembles discontinuous or first-order phase-transition. At the same time, the correlation length and specific heat exhibit astonishing strong sharp peaks quite similar to a second-order phase-transition. We associate the ascending and descending parts of the peak with power-law “pseudo-critical” exponents. We determine the pseudo-critical exponents in the temperature range where these peaks are developed, namely, $\nu = 1$ for the correlation length and $\alpha = 3$ for the specific heat. We also study the behavior of the electron density and isothermal compressibility around the pseudo-critical temperature.

DOI: [10.1103/PhysRevE.103.042123](https://doi.org/10.1103/PhysRevE.103.042123)**I. INTRODUCTION**

In recent investigations of several decorated one-dimensional models with short-range interactions, the first derivative of free energy, such as entropy, internal energy, and magnetization, shows a steplike function of temperature but still with a continuous change which is quite similar to a first-order phase transition behavior. The second-order derivative of free energy, such as the specific heat and magnetic susceptibility, resembles a typical second-order phase transition behavior at finite temperature. This peculiar behavior drew attention to a more careful study, as considered in Ref. [1]. In Ref. [2], an additional discussion of the above phenomenology focused in the behavior of the correlation function for arbitrarily distant spins around the pseudo-transition. Similar pseudo-transitions were shown to take place in the Ising-Heisenberg diamond chain [3,4] and even in the pure Ising diamond chain [5]. It also has been explored in the one-dimensional double-tetrahedral model where the nodal sites are occupied by localized Ising spins and alternate with a pair of delocalized mobile electrons within a triangular plaquette [6]. Similarly, the ladder model with alternating Ising-Heisenberg coupling [7] as well as the triangular tube model with Ising-Heisenberg coupling [8] depict pseudo-transition signatures. A universal character of preasymptotic pseudo-critical exponents has been demonstrated [9,10]. These pseudo-transitions taking place at finite temperatures in one-dimensional model systems with

short-range interactions are of a distinct nature from the true phase-transition exhibited in the presence of long-range couplings for which the correlation length diverges, but, e.g., the specific heat can be without divergence [11]. In all the above model systems presenting a pseudo-transition at finite temperature, one of the couplings was assumed to be Ising-like in order to allow for the exact calculation of the thermodynamic quantities. Examples of pseudo-transitions taking place in one-dimensional systems of interacting electrons without the assumption of an Ising-like nature of relevant couplings are still missing.

The Hubbard model is one of the simplest models that describe more accurately strongly interacting electron systems, which have attracted a great deal of interest over the past decades related to the possible emergence of geometrical frustration properties [12,13]. Magnetic frustration in highly correlated electron models arises due to the geometric structure of the lattice, which induces system failures to satisfy simultaneously conflicting local requirements. The geometric frustration of the Hubbard model has been extensively studied, particularly, in the diamond chain structure as considered by Derzhko and co-workers [14–16] where frustration for a particular class of lattice was discussed. Montenegro-Filho and Coutinho-Filho [17] also considered the doped AB_2 Hubbard chain both in the weak coupling and in the infinite- U limit (atomic limit) where quite interesting phases were identified as a function of hole doping away

from the half-filled band as well as 1/3-plateau magnetization, Kosterlitz-Thouless transition, and Luttinger liquid [18]. Furthermore, Gulacsi *et al.* [19] also discussed the diamond Hubbard chain in a magnetic field and a wide range of properties, such as flatband ferromagnetism, correlation-induced metallic, and half-metallic processes. The thermodynamics of the Hubbard model on a diamond chain in the atomic limit was discussed in Ref. [20]. Furthermore, frustrated quantum Heisenberg double-tetrahedral and octahedral chains at high magnetic fields was discussed in Ref. [21]. Fermionic entanglement due to spin frustration was investigated in the hybrid diamond chain with localized Ising spins and mobile electrons [22].

On the other hand, generally rigorous analysis of the Hubbard model is a challenging task. Only in a particular case it is possible to obtain exact results [23]. Earlier in the 1970s, Beni and Pincus [24] focused in the one-dimensional Hubbard model. Later Mancini [25] and Mancini and Mancini [26] discussed several additional properties of the extended one-dimensional Hubbard model in the atomic limit, obtaining the chemical potentials plateaus of the particle density as a function of the on-site Coulomb potential at zero temperature. Earlier, the spinless versions of the Hubbard model on the diamond chain also was investigated [27] as well as Lopes and Dias [28] performed a detailed investigation using the exact diagonalization approach. The Ising-Hubbard diamond chain has been investigated in Ref. [29]. In addition, experimental data regarding the 1/3 magnetization plateau in azurite [30,31] were reproduced in several theoretical model systems, such as the Ising-Heisenberg diamond chain [32–34]. The quantum block-block entanglement was investigated in the one-dimensional extended Hubbard model by exact diagonalization [35]. When the absolute value of the nearest-neighbor Coulomb interaction becomes small, the effects of the hopping term and the on-site interaction cannot be neglected. The experimental observation of the double peaks both in the magnetic susceptibility and specific heat [36–38] can be described accurately by the extended Hubbard diamond chain model without the hopping of electrons or holes between the nodal sites. The interplay between interactions and magnetic flux in the electronic properties of two-body and many-body Hubbard diamond chains were also investigated showing a diversity of unconventional physical properties [19,39,40].

From an experimental point of view, the diamond chain structure is also motivating. Recently, the compound $\text{Cu}_3(\text{CH}_3\text{COO})_4(\text{OH})_5 \cdot 5\text{H}_2\text{O}$ has been synthesized [41], which exhibits a unique one-dimensional diamond chain structure. The well known natural mineral azurite $\text{Cu}_3(\text{CO}_3)_2(\text{OH})_2$ [37] is also well represented by a similar diamond chain geometry. These and similar compounds would be ideal physical systems on which pseudotransitions at finite temperature could be searched.

Here, we advance in the study of pseudo-phase-transitions in quasi one-dimensional systems by presenting a detailed exact study of the thermodynamic properties of the diamond chain Hubbard model in the atomic limit. The present article is organized as follows: In Sec. II, we revisit the extended Hubbard model on the diamond chain structure [20] with

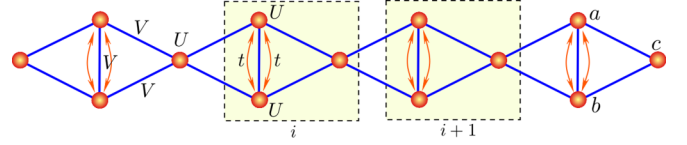


FIG. 1. Schematic of the extended Hubbard model on the diamond chain. The on-site Coulomb repulsion interaction is denoted by U , and nearest-neighbor repulsion interaction is represented by V and V_1 , t stands for the electron hopping term.

nodal sites considered in the atomic limit. In Sec. III we present our main findings where we focus in the existence of a pseudo-critical temperature by exploring the behavior of the correlation length. In Sec. IV (Sec. V) we analyze first (second) derivative physical quantities in the vicinity of the pseudo-transition. Finally, Sec. VI is devoted to our conclusions and perspectives.

II. THE EXTENDED HUBBARD MODEL

In this section, we revisit the model considered in Ref. [20]. Some results that will be used in the following section are updated and summarized. The model illustrated in Fig. 1, consider the hopping term t between sites a and b . Additionally, there is an on-site Coulomb repulsion interaction U and nearest-neighbor repulsion interaction V between a and b , whereas V_1 corresponds the coupling between of nodal sites c with sites a and b (as labeled in the last block of Fig. 1). We also assume that this model has an arbitrary particle density. Thus, the system will be described by including a chemical potential denoted by μ . The Hamiltonian of the proposed model can be expressed by

$$\mathbf{H} = \sum_{i=1}^N \mathbf{H}_{i,i+1}, \quad (1)$$

with N being the number of unit cells (sites a – c), and $\mathbf{H}_{i,i+1}$ is given by

$$\begin{aligned} \mathbf{H}_{i,i+1} = & -t \sum_{\sigma=\downarrow,\uparrow} (\mathbf{a}_{i,\sigma}^\dagger \mathbf{b}_{i,\sigma} + \mathbf{b}_{i,\sigma}^\dagger \mathbf{a}_{i,\sigma}) - \mu (\mathbf{n}_i^a + \mathbf{n}_i^b + \mathbf{n}_i^c) \\ & + U (\mathbf{n}_{i,\uparrow}^a \mathbf{n}_{i,\downarrow}^a + \mathbf{n}_{i,\uparrow}^b \mathbf{n}_{i,\downarrow}^b + \mathbf{n}_{i,\uparrow}^c \mathbf{n}_{i,\downarrow}^c) \\ & + V \mathbf{n}_i^a \mathbf{n}_i^b + V_1 (\mathbf{n}_i^a + \mathbf{n}_i^b) (\mathbf{n}_i^c + \mathbf{n}_{i+1}^c), \end{aligned} \quad (2)$$

with $\mathbf{a}_{i,\sigma}$, and $\mathbf{b}_{i,\sigma}$ ($\mathbf{a}_{i,\sigma}^\dagger$ and $\mathbf{b}_{i,\sigma}^\dagger$) being the Fermi annihilation (creation) operators for electrons, whereas σ stands for the electron spin and $\mathbf{n}_{i,\sigma}^\alpha$ stands for the number operator with $\alpha = \{a, b, c\}$. Using this number operator, we also define conveniently the following operators $\mathbf{n}_i^\alpha = \mathbf{n}_{i,\uparrow}^\alpha + \mathbf{n}_{i,\downarrow}^\alpha$.

In order to contract and to symmetrize the Hamiltonian (2), we can define properly the following operators:

$$\begin{aligned} \mathbf{p}_{i,i+1} &= \frac{1}{2} (\mathbf{n}_i^c + \mathbf{n}_{i+1}^c), \\ \mathbf{q}_{i,i+1} &= \frac{1}{2} (\mathbf{n}_{i,\uparrow}^c \mathbf{n}_{i,\downarrow}^c + \mathbf{n}_{i+1,\uparrow}^c \mathbf{n}_{i+1,\downarrow}^c). \end{aligned} \quad (3)$$

TABLE I. The first column means the number of particles in dimer plaquette, the second column describes the dimer plaquette magnetization, the third column reports the eigenvalues, whereas the fourth column corresponds to the eigenvalues degeneracy. The fifth column corresponds to the eigenvectors of dimer plaquette. Here $\mathbf{D}_m = -(\mu - 2V_1 \mathbf{p}_{i,i+1})m - \mu \mathbf{p}_{i,i+1} + U \mathbf{q}_{i,i+1}$ and $\cot(2\theta) = \frac{U-V}{4t}$.

m	M_{ab}	Eigenvalues	g	Eigenvectors
0	0	$\lambda_{0,0} = \mathbf{D}_0$,	1	$ \mathcal{S}_{00}\rangle = 0\rangle$
1	0.5	$\lambda_{0,\sigma}^{(\pm)} = \mathbf{D}_1 \pm t$	2	$ \mathcal{S}_{0\sigma}^{(\pm)}\rangle = \frac{1}{\sqrt{2}}(0\rangle \mp \sigma\rangle)$
2	1	$\lambda_{\sigma,\sigma} = \mathbf{D}_2 + V$	2	$ \mathcal{S}_{\sigma\sigma}\rangle = \sigma\rangle$
	0	$\lambda_{0,\parallel}^{(1)} = \mathbf{D}_2 + U$	1	$ \mathcal{S}_{0,\parallel}^{(1)}\rangle = \frac{1}{\sqrt{2}}(0\rangle - \parallel\rangle)$
	0	$\lambda_{\uparrow\uparrow}^{(+)} = \mathbf{D}_2 + V + 2t \cot(\theta)$	1	$ \mathcal{S}_{\uparrow\uparrow}^{(+)}\rangle = \frac{1}{\sqrt{2}}\{\cos(\theta)(\parallel\rangle + \uparrow\rangle) - \sin(\theta)(\downarrow\rangle + \uparrow\rangle)\}$
	0	$\lambda_{\uparrow\uparrow}^{(-)} = \mathbf{D}_2 + V - 2t \tan(\theta)$	1	$ \mathcal{S}_{\uparrow\uparrow}^{(-)}\rangle = \frac{1}{\sqrt{2}}\{\sin(\theta)(\parallel\rangle + \uparrow\rangle) + \cos(\theta)(\downarrow\rangle + \uparrow\rangle)\}$
	0	$\lambda_{\downarrow,\uparrow}^{(2)} = \mathbf{D}_2 + V$	1	$ \mathcal{S}_{\downarrow,\uparrow}^{(2)}\rangle = \frac{1}{\sqrt{2}}(\downarrow\rangle - \uparrow\rangle)$
3	0.5	$\lambda_{\parallel,\sigma}^{(\pm)} = \mathbf{D}_3 + U + 2V \pm t$	2	$ \mathcal{S}_{\parallel,\sigma}^{(\pm)}\rangle = \frac{1}{\sqrt{2}}(\sigma\rangle \mp \parallel\rangle)$
4	0	$\lambda_{\parallel,\parallel} = \mathbf{D}_4 + 2U + 4V$	1	$ \mathcal{S}_{\parallel,\parallel}\rangle = \parallel\rangle$

Using these operators, we can rewrite the Hamiltonian (2), which becomes as follows:

$$\begin{aligned}
 \mathbf{H}_{i,i+1} = & -t \sum_{\sigma=\downarrow,\uparrow} (\mathbf{a}_{i,\sigma}^\dagger \mathbf{b}_{i,\sigma} + \mathbf{b}_{i,\sigma}^\dagger \mathbf{a}_{i,\sigma}) - \mu \mathbf{p}_{i,i+1} \\
 & - (\mu - 2V_1 \mathbf{p}_{i,i+1})(\mathbf{n}_i^a + \mathbf{n}_i^b) + V \mathbf{n}_i^a \mathbf{n}_i^b \\
 & + U (\mathbf{n}_{i,\uparrow}^a \mathbf{n}_{i,\downarrow}^a + \mathbf{n}_{i,\uparrow}^b \mathbf{n}_{i,\downarrow}^b) + U \mathbf{q}_{i,i+1}. \quad (4)
 \end{aligned}$$

It is worth mentioning that this model already was investigated in Ref. [20] for an arbitrary number of electrons. Here we consider in each site the following basis $\{0, \uparrow, \downarrow, \parallel\}$.

The eigenvalues and eigenvectors of the dimer plaquette are summarized in Table I, which are valid, in general, for arbitrary values of the Hamiltonian (1) parameters.

It is worth mentioning that all analyses performed throughout this paper will be performed in the thermodynamic limit. Finite size effects can be evaluated in a similar way to that put forward in Ref. [42].

A. Phase diagram

In order to analyze some relevant features, we will focus on the more interesting case when the particle-hole symmetry is satisfied which follows the restriction $V_1 = V/2$. Under this condition, for instance, we can analyze the half-filled band case, which occurs under the following restriction for the chemical potential $\mu = U/2 + 2V$.

It is worthy to mention that, the Hamiltonian (2), has 64 eigenvalues per diamond plaquette. The zero temperature phase diagram analysis was already discussed in Ref. [20]. Below we just give some ground-state energies relevant to the following analysis of the pseudo-transition features. In what follows, we will consider all energies in units of U .

Figure 2(a) illustrates the zero temperature phase diagram on the plane t - μ for fixed $V/U = 0.1$ and $0 < \mu/U < 0.3$. There is a phase corresponding to a dimer antiferromagnetic

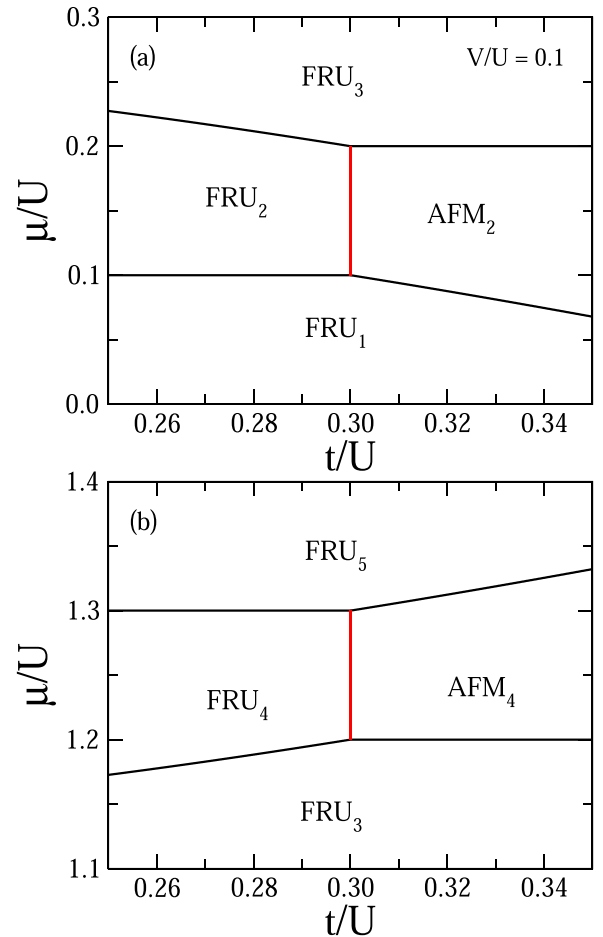


FIG. 2. Zero temperature phase diagram on the plane t - μ , assuming fixed $V/U = 0.1$. (a) Shows the region of μ/U values where $\rho = 2/3$ phases appear; (b) the range of μ/U values where $\rho = 4/3$ phases appear.

(AFM₂) state,

$$|\text{AFM}_2\rangle = \prod_{i=1}^N |S_{i\pm}^{(-)}\rangle |0\rangle. \quad (5)$$

In this case, there are two electrons with opposite spins in the dimer sites, whereas nodal sites are empty. Thus, the electron density per unit cell is $\rho = 2/3$. The corresponding eigenvalue is given by

$$E_{\text{AFM}_2} = -2\mu + V - 2t \tan(\theta). \quad (6)$$

There is also a phase corresponding to a dimer and nodal frustrated (FRU₂) state,

$$|\text{FRU}_2\rangle = \prod_{i=1}^N \frac{1}{\sqrt{2}} \left(\begin{array}{c} |0\rangle \\ |\sigma_i\rangle \end{array} - \begin{array}{c} |\sigma_i\rangle \\ |0\rangle \end{array} \right) |\tau_i\rangle. \quad (7)$$

This state also has two electrons: One electron is in a dimer site whereas the other occupies a nodal site both with arbitrary spin orientation. The electron density $\rho = 2/3$. The corresponding residual entropy in units of k_B is $\mathcal{S} = \ln(4)$, whereas the ground-state energy becomes

$$E_{\text{FRU}_2} = -2\mu - t + V. \quad (8)$$

The vertical red line corresponds to $t_c = (U - V)/3 = 0.3U$. We will focus in this phase boundary between $|\text{AFM}_2\rangle$ and $|\text{FRU}_2\rangle$. The corresponding interface residual entropy is $\mathcal{S} = k_B \ln(4)$, as we will verify ahead.

Other surrounding states in the phase diagram are as follows:

$$|\text{FRU}_1\rangle = \prod_{i=1}^N \frac{1}{\sqrt{2}} \left(\begin{array}{c} |\sigma\rangle \\ |0\rangle \end{array} - \begin{array}{c} |0\rangle \\ |\sigma\rangle \end{array} \right) |0\rangle, \quad (9)$$

with $n = 1$ particle per unit cell and electron density $\rho = 1/3$,

$$|\text{FRU}_3\rangle = \prod_{i=1}^N \frac{1}{\sqrt{2}} \left(\begin{array}{c} |\uparrow\rangle \\ |0\rangle \end{array} - \begin{array}{c} |0\rangle \\ |\uparrow\rangle \end{array} \right) |\tau_i\rangle, \quad (10)$$

with $n = 3$ electrons per unit cell or $\rho = 1$. The residual entropy in the frustrated phases (9) and (10) is given by $\mathcal{S} = k_B \ln(2)$.

Similarly, in Fig. 2(b) we show the phase diagram for the same set of fixed parameters but in the range $1.1 < \mu/U < 1.4$ where $\rho = 4/3$ phases appear.

In this region we observe also another dimer antiferromagnetic (AFM₄) state given by

$$|\text{AFM}_4\rangle = \prod_{i=1}^N |S_{i\pm}^{(-)}\rangle |\uparrow\rangle, \quad (11)$$

where two electrons with opposite spins are located in the dimer sites, and the other pair of electrons is located in the nodal site. The respective ground-state energy becomes

$$E_{\text{AFM}_4} = -4\mu + 5V + U - 2t \tan(\theta). \quad (12)$$

There is also a dimer and nodal frustrated state (FRU₄),

$$|\text{FRU}_4\rangle = \prod_{i=1}^N \frac{1}{\sqrt{2}} \left(\begin{array}{c} |\uparrow\rangle \\ |\sigma_i\rangle \end{array} - \begin{array}{c} |\sigma_i\rangle \\ |\uparrow\rangle \end{array} \right) |\tau_i\rangle, \quad (13)$$

with corresponding ground-state energy,

$$E_{\text{FRU}_4} = -4\mu - t + 5V + U, \quad (14)$$

and electron density $\rho = 4/3$.

The vertical red line corresponds to $t = (U - V)/3 = 0.3U$ which gives the phase boundary between $|\text{AFM}_4\rangle$ and $|\text{FRU}_4\rangle$ on which the residual entropy is $\mathcal{S} = k_B \ln(4)$ as we will verify ahead.

The additional phase states illustrated in this diagram is composed by $n = 5$,

$$|\text{FRU}_5\rangle = \prod_{i=1}^N \frac{1}{\sqrt{2}} \left(\begin{array}{c} |\uparrow\rangle \\ |\sigma_i\rangle \end{array} - \begin{array}{c} |\sigma_i\rangle \\ |\uparrow\rangle \end{array} \right) |\uparrow\rangle, \quad (15)$$

with $\rho = 5/3$. This frustrated phase has residual entropy $\mathcal{S} = k_B \ln(2)$.

Further details of the ground-state phase diagrams can be found in Ref. [20]. Pseudo-transitions are identified in the close vicinity of the AFM₂ – FRU₂ and the AFM₄ – FRU₄ phase boundaries.

B. Thermodynamics

In order to use the decoration transformation approach, we need to write the sum of the Boltzmann factors connecting the nodal sites i and $i + 1$ with each possible occupation configuration for the extended Hubbard model on the diamond chain. These can be written as follows:

$$\begin{aligned} w_{n_i^c, n_{i+1}^c} = & e^{-\beta D_0} + 4(e^{-\beta D_1} + e^{-\beta(D_3+U+2V)}) \cosh(\beta t) \\ & + e^{-\beta D_2}(e^{-\beta U} + 3e^{-\beta V}) + e^{-\beta(D_4+2U+4V)} \\ & + e^{-\beta(D_2+V)}(e^{-\beta \vartheta_+ t/2} + e^{-\beta \vartheta_- t/2}), \end{aligned} \quad (16)$$

with $\beta = 1/k_B T$ and

$$D_m = -(\mu - V \mathbf{p}_{i,i+1})m - \mu \mathbf{p}_{i,i+1} + U \mathbf{q}_{i,i+1}. \quad (17)$$

Here, ϑ_{\pm} is defined by

$$\vartheta_{\pm} = \frac{U - V \pm \sqrt{(U - V)^2 + 16t^2}}{t}. \quad (18)$$

To solve the effective Hubbard model with up to four-body coupling, we can use the transfer matrix method [43], similar to that used in Refs. [24,27]. Therefore, the symmetric Hamiltonian by exchanging $i \rightarrow i + 1$ and $i + 1 \rightarrow i$ leads to a symmetric transfer matrix which can be expressed by

$$\mathbf{W} = \begin{bmatrix} w_{0,0} & w_{0,1} & w_{0,1} & w_{0,2} \\ w_{0,1} & w_{1,1} & w_{1,1} & w_{1,2} \\ w_{0,1} & w_{1,1} & w_{1,1} & w_{1,2} \\ w_{0,2} & w_{1,2} & w_{1,2} & w_{2,2} \end{bmatrix}, \quad (19)$$

where the elements of \mathbf{W} are given by Eq. (15). Let us define a convenient notation,

$$\begin{aligned} w_{0,0}(x) = & 1 + 2x \left(1 + \frac{x^2}{z^4 y^2} \right) \left(\frac{1}{\gamma^2} + \gamma^2 \right) \\ & + x^2 \left(\frac{3}{z^2} + \frac{1}{y^2} + \frac{1}{yz\zeta} + \frac{\zeta}{yz} \right) + \frac{x^4}{y^4 z^8}, \end{aligned} \quad (20)$$

with $x = e^{\beta \mu}$, $y = e^{(1/2)\beta U}$, $z = e^{(1/2)\beta V}$, $\gamma = e^{(1/2)\beta t}$, and $\zeta = e^{(1/2)\beta \sqrt{(U-V)^2 + 16t^2}}$. All other Boltzmann factors could be

TABLE II. Cubic root solutions are tabulated in decreasing order by intervals in ϕ .

ϕ	Largest	Second largest	Lowest
$(0, \pi)$	Λ_0	Λ_1	Λ_2
$(\pi, 2\pi)$	Λ_1	Λ_0	Λ_2
$(2\pi, 3\pi)$	Λ_1	Λ_2	Λ_0
$(3\pi, 4\pi)$	Λ_2	Λ_1	Λ_0
$(4\pi, 5\pi)$	Λ_2	Λ_0	Λ_1
$(5\pi, 6\pi)$	Λ_0	Λ_2	Λ_1

expressed in terms of $w_{0,0}(x)$ defined by Eq. (20) as follows:

$$w_{n_1, n_2}(x) = \frac{x^{(n_1+n_2)/2}}{y^{\lfloor n_1/2 \rfloor + \lfloor n_2/2 \rfloor}} w_{0,0}\left(\frac{x}{z^{n_1+n_2}}\right), \quad (21)$$

by $\lfloor \dots \rfloor$ we mean the floor function for any real number.

In order to carry out a reduced transfer matrix, we use the symmetry of the system. The proposed Hamiltonian is invariant with respect to electron spin orientation in nodal sites (site c). Therefore, the reduced transfer matrix becomes

$$\mathbf{V} = \begin{bmatrix} w_{0,0} & \sqrt{2} w_{0,1} & w_{0,2} \\ \sqrt{2} w_{0,1} & 2 w_{1,1} & \sqrt{2} w_{1,2} \\ w_{0,2} & \sqrt{2} w_{1,2} & w_{2,2} \end{bmatrix}. \quad (22)$$

The determinant of the reduced transfer matrix becomes a cubic equation of the form

$$\det(\mathbf{V} - \Lambda) = (\Lambda^3 + a_3 \Lambda^2 + a_2 \Lambda + a_1) = 0, \quad (23)$$

where the coefficients become

$$\begin{aligned} a_1 &= 2w_{0,0}w_{1,2}^2 + 2w_{0,2}^2w_{1,1} + 2w_{0,1}^2w_{2,2} \\ &\quad - 2w_{0,0}w_{1,1}w_{2,2} - 4w_{0,2}w_{0,1}w_{1,2}, \\ a_2 &= 2w_{0,0}w_{1,1} + 2w_{1,1}w_{2,2} + w_{0,0}w_{2,2} \\ &\quad - 2w_{0,1}^2 - w_{0,2}^2 - 2w_{1,2}^2, \\ a_3 &= -w_{0,0} - 2w_{1,1} - w_{2,2}. \end{aligned} \quad (24)$$

Consequently, the roots of the algebraic cubic equation may be expressed as follows:

$$\Lambda_j = 2\sqrt{Q} \cos\left(\frac{\phi - 2\pi j}{3}\right) - \frac{1}{3}a_3, \quad j = \{0, 1, 2\}, \quad (25)$$

with

$$\phi = \arccos\left(\frac{R}{\sqrt{Q^3}}\right), \quad (26)$$

$$Q = \frac{a_3^2 - 3a_2}{9}, \quad (27)$$

$$R = \frac{9a_2a_3 - 27a_1 - 2a_3^3}{54}. \quad (28)$$

It is verified that $Q > 0$ in Appendix A, which implies that all three roots must be different and real. We also analyze which eigenvalues must be the largest and the lowest one. So, it is enough to restrict $0 < \phi < \pi$ in the cubic solution without losing its general solution as discussed in Appendix A. Other intervals just exchange the cubic root solutions as illustrated

in Table II. In the interval $0 < \phi < \pi$, the eigenvalues are ordered as $\Lambda_0 > \Lambda_1 > \Lambda_2$.

III. PSEUDO-CRITICAL TEMPERATURE

In this section we will analyze the anomalous thermodynamic property of the present extended diamond chain Hubbard model in the atomic limit [20]. In order to study the thermodynamic properties, we will use the exact free energy $f = -\frac{1}{\beta} \ln(\Lambda_0)$ as a starting point. Therefore, we will proceed our discussion of thermodynamic properties as a function of temperature and chemical potential. Particularly, we will analyze entropy, internal energy, correlation length, specific heat, electron density, and isothermal compressibility. We aim to study physical quantities around the pseudo-critical temperature T_p . We stress that the present definition of pseudo-critical is different from that defined by Saito [44] to describe the critical-like behavior in approaching the spinodal point near the first-order transition. Therefore, by using a perturbation approach, we can find the eigenvalues of transfer matrix (22), as discussed in Appendix B.

In general, pseudo-transitions can be manipulated and analyzed using perturbation techniques as detailed in Appendix B. For this purpose, we consider as unperturbed matrix \mathbf{V}_0 defined in Appendix Eq. (B1). The eigenvalues of the matrix (B1), are given by (B2)–(B4) where we can observe the largest and second-largest eigenvalues are given by (B2) and (B3), respectively.

In the low temperature region we have the condition $w_{0,2} \ll \{w_{0,0}, w_{1,1}, w_{2,2}\}$. This is so because each matrix element results from the sum of the Boltzmann factors corresponding to all eigenstates of the unit cell with a specific configuration of the nodal sites. Therefore, the leading term of $w_{0,2}$ comes from the lowest energy contribution to $w_{0,2}$ that includes only excited states, namely, E_e , whereas the leading terms of $w_{0,0}$, $w_{1,1}$, and $w_{2,2}$ are given by the corresponding ground states within each specific nodal sites configuration. Therefore, in the low temperature regime and physical parameters close to the ground-state boundary line between the AFM₂ and the FRU₂ phases $w_{0,2}/w_{0,0} \propto e^{-(E_e - E_{\text{AFM}_2})/k_B T}$ and $w_{0,2}/w_{1,1} \propto e^{-(E_e - E_{\text{FRU}_2})/k_B T}$ become exponentially small. Similar relations hold among $w_{0,2}$, $w_{1,1}$, and $w_{2,2}$ in the close vicinity of the AFM₄ – FRU₄ ground-state boundary line.

When (B2) and (B3) become eventually equal, we can get a pseudo-critical temperature from (B5), which reads

$$u_0^{(0)} = u_1^{(0)}. \quad (29)$$

Similar as discussed in Ref. [1], the relation (29) can induce us to believe that there is a true phase-transition at finite temperature. However, the condition (29) does not mean that the transfer matrix eigenvalues satisfy $\Lambda_0 = \Lambda_1$: The condition (29) is satisfied only when the matrix (B8) is ignored and for $w_{0,2} = 0$. Therefore, the first-order perturbative corrections [see Eqs. (B9) and (B11)] are $u_0^{(1)} > 0$ and $u_1^{(1)} < 0$, which implies that the approximate solution given in (B12) must satisfy $\Lambda_0 > \Lambda_1$.

Returning to the relation (29), we get the following equation:

$$w_{0,0} = 2w_{1,1} \quad \text{for } w_{0,0} > w_{2,2}, \quad (30)$$

and this one corresponds to the vicinity of the boundary line between AFM₂ and FRU₂.

The asymptotic behavior of T_p as the hopping parameter t approaches the critical value $t_c = (U - V)/3$ (the boundary between the AFM₂ and the FRU₂ phases) can be analytically demonstrated by noting that, in the low temperature regime, these two possible ground states give the dominant contributions to the sum of Boltzmann factors on $w_{0,0}$ and $w_{1,1}$. It is important to stress that, whereas there is a single AFM₂ state, the FRU₂ state is degenerated. Therefore, at low temperatures, Eq. (30) defining the pseudo-critical temperature assumes the asymptotic form

$$e^{-E_{\text{AFM}_2}/k_B T_p} = 4e^{-E_{\text{FRU}_2}/k_B T_p}, \quad (31)$$

from which we have $k_B T_p = \Delta E / \ln 4$ where $\Delta E = E_{\text{FRU}_2} - E_{\text{FRU}_4} = 2t \tan \theta - t$ with $\cot 2\theta = (U - V)/4t$ (see Table I). For hopping amplitudes t in the close vicinity of the boundary line separating these two ground states [given by $\tan \theta_c = 1/2$ or, equivalently, $\tan 2\theta_c = 4/3$ or $t_c = (U - V)/3$], the first-order contribution in $(t - t_c)$ to the energy gap can be shown to be given by $\Delta E = (3/5)(t - t_c)$ [for this we considered $\tan 2\theta = 4/3 + 4(t - t_c)/3t_c$ which, up to first order, corresponds to $\tan \theta = 1/2 + 3(t - t_c)/10t_c$]. According to the above lines, the pseudo-critical temperature is found to decrease as

$$k_B T_p = 3(t - t_c)/10 \ln 2, \quad (32)$$

when t approaches t_c from above.

Similarly, the relation (29) leads to the following equation:

$$w_{2,2} = 2w_{1,1} \quad \text{for } w_{0,0} < w_{2,2}, \quad (33)$$

which holds in the close vicinity of the FRU₄ - AFM₄ boundary line. The asymptotic behavior of T_p in this regime assumes the same expression derived above.

In Fig. 3(a), we illustrate the pseudo-critical temperature T_p as a function of chemical potential μ . The continuous line corresponds to the pseudo-transition that occurs at low chemical potentials for which there are nearly two electrons per unit cell (near the boundary between AFM₂ and FRU₂ phases). The dashed line accounts for the second pseudo-transition appearing at larger chemical potential for which there are four electrons per unit cell in the ground state (near the boundary between AFM₄ and FRU₄ phases). In this latter case, the chemical potential was conveniently shifted to $(\mu - V - U)/U = \mu/U - 1.1$ (top scale) to allow representing both pseudo-transitions in the same frame.

In panel (b) the pseudo-critical temperatures T_p as a function of t/U for $\mu/U = 0.18$ (solid red line) and $\mu/U = 1.28$ (dashed blue line) are reported. The pseudo-critical temperature vanishes linearly $T_p \propto (t - t_c)$ as the boundary line $t_c = (U - V)/3$ is approached from above, i.e., within one of the AFM ground states. The dashed-dot line corresponds to the asymptotic analytical expression Eq. (32), in perfect agreement with the numerical data.

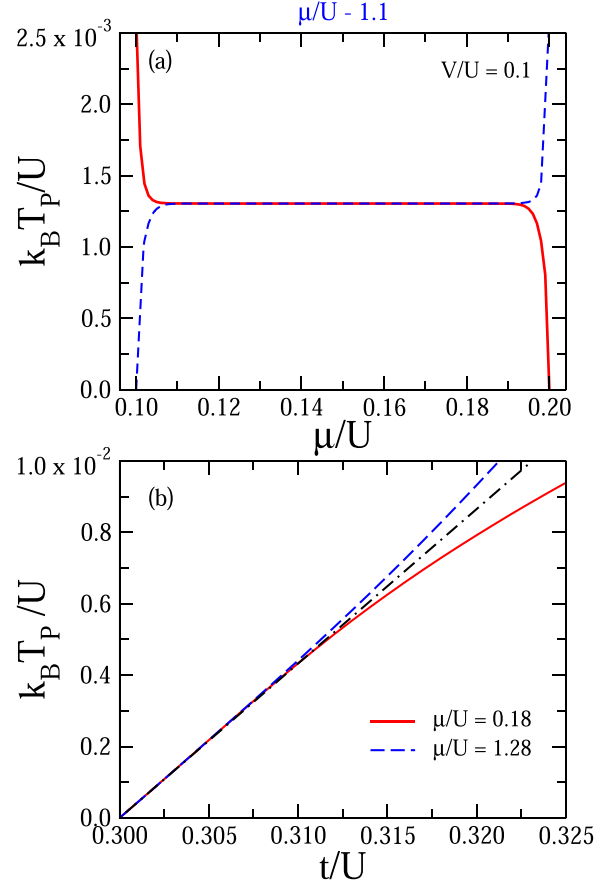


FIG. 3. (a) Pseudo-critical temperature T_p for fixed parameters $t/U = 0.303$ and $V/U = 0.1$ near AFM₂ and FRU₂ phase boundaries (solid line) and near the AFM₄ and FRU₄ phase boundaries (dashed line). In the latter the chemical potential was shifted to $(\mu - U - V)/U = \mu/U - 1.1$ with values shown on the top scale. (b) Pseudo-critical temperature T_p as a function of t/U for $\mu/U = 0.18$ (solid red line) and $\mu/U = 1.28$ (dashed blue line). The dashed-dot line corresponds to the analytic asymptotic behavior Eq. (32).

A. Correlation length

Since the eigenvalues are nondegenerate, the correlation length ξ can be obtained by using the largest Λ_0 and second largest Λ_1 eigenvalues given from (25). It is simply written as

$$\xi = \left[\ln \left(\frac{\Lambda_0}{\Lambda_1} \right) \right]^{-1}. \quad (34)$$

In Fig. 4 we illustrate the correlation length as a function of temperature. Panel (a) reports data for several values of t/U and assuming fixed $\mu/U = 0.18$ and $V/U = 0.1$. Here we observe how the peak becomes more pronounced when $t \rightarrow t_c = (U - V)/3 = 0.3U$ (approaching the FRU₂ - AFM₂ ground-state phase boundary). For larger t the height of the peak becomes lower and broader. For $t/U = 0.303$ we already observe a strong peak around T_p , which was computed with high precision to be $k_B T_p / U = 1.304\,618\,413\,6496 \times 10^{-3}$. Similarly, panel (b) reports for the same parameters set used in (a) but for $\mu/U = 1.28$ (in the vicinity of the FRU₄ - AFM₄ phase boundary).

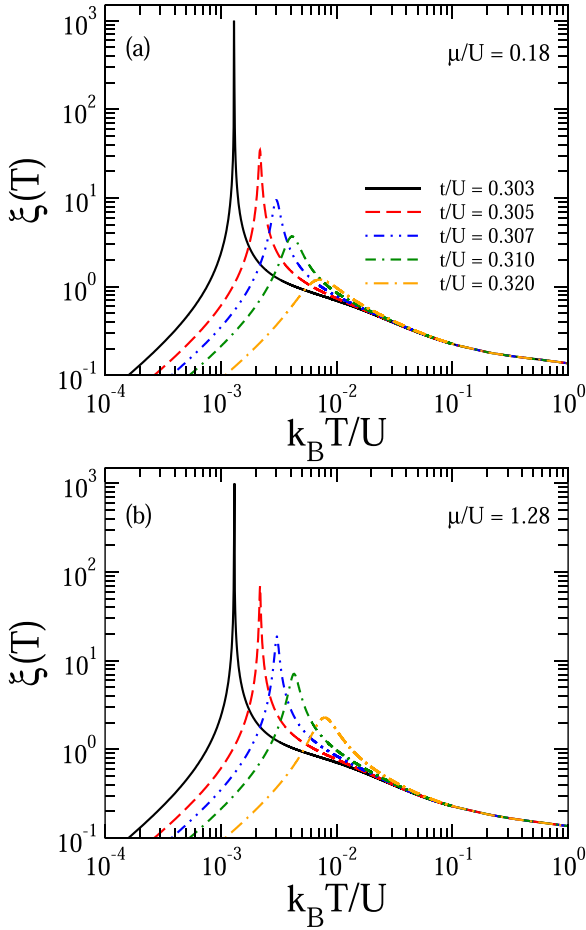


FIG. 4. Correlation length as a function of temperature on the logarithmic scale for $V/U = 0.1$. (a) For several values of t and fixed $\mu/U = 0.18$ (in the vicinity of the $\text{FRU}_2 - \text{AFM}_2$ phase boundary). (b) For several values of t and fixed $\mu/U = 1.28$ (in the vicinity of the $\text{FRU}_4 - \text{AFM}_4$ phase boundary).

There are two situations where pseudo-transition occurs. The first one satisfies the condition $w_{0,0} \sim 2w_{1,1}$ but in the perturbation regime for which $8w_{0,1}^2 \ll (w_{0,0} - 2w_{1,1})^2$. Under this condition, we have the following result:

$$\frac{\Lambda_0}{\Lambda_1} \rightarrow \begin{cases} \frac{w_{0,0}}{2w_{1,1}}, & w_{0,0} > 2w_{1,1}, \\ \frac{2w_{1,1}}{w_{0,0}}, & w_{0,0} < 2w_{1,1}. \end{cases} \quad (35)$$

Consequently, in the regime where the perturbation approach stands, the correlation length in the close vicinity of the pseudo-critical temperature can be expressed by

$$\xi_0(\tau) = c_{0,\xi} |\tau|^{-1} + O(\tau^0). \quad (36)$$

Here $\tau = (T - T_p)/T_p$, and the coefficient is given by

$$c_{0,\xi} = \frac{\tilde{w}_{0,0}}{T_p \tilde{v}_0}, \quad (37)$$

with $\tilde{w}_{0,0}$ is $w_{0,0}$ evaluated at $T = T_p$, and

$$\tilde{v}_0 = \left| \frac{\partial(w_{0,0} - 2w_{1,1})}{\partial T} \right|_{T_p}. \quad (38)$$

Note that $w_{0,0}(T_p)$ remains finite at $T_p \neq 0$ because it is the sum of positive Boltzmann factors. Furthermore, whereas $w_{0,0} - 2w_{1,1} = 0$ at T_p , its derivative is non-null. Therefore, the coefficient $c_{0,\xi}$ remains finite at T_p as confirmed numerically.

Similarly, the second pseudo-transition occurs when $w_{2,2} \sim 2w_{1,1}$ but in the perturbation regime $8w_{1,2}^2 \ll (w_{2,2} - 2w_{1,1})^2$, that provides us,

$$\frac{\Lambda_0}{\Lambda_1} \rightarrow \begin{cases} \frac{w_{2,2}}{2w_{1,1}}, & w_{2,2} > 2w_{1,1}, \\ \frac{2w_{1,1}}{w_{2,2}}, & w_{2,2} < 2w_{1,1}. \end{cases} \quad (39)$$

Analogously, the correlation length close to the pseudo-transition, can be expressed around T_p , resulting in

$$\xi_2(\tau) = c_{2,\xi} |\tau|^{-1} + O(\tau^0), \quad (40)$$

where the coefficient is given by

$$c_{2,\xi} = \frac{\tilde{w}_{2,2}}{T_p \tilde{v}_2}, \quad (41)$$

with $\tilde{w}_{2,2}$ evaluated at $T = T_p$, and

$$\tilde{v}_2 = \left| \frac{\partial(w_{2,2} - 2w_{1,1})}{\partial T} \right|_{T_p}. \quad (42)$$

$c_{2,\xi}$ is also predicted to remain finite at T_p as confirmed numerically. These preasymptotic power laws fail for very small τ because the perturbation conditions cannot be satisfied at T_p . Therefore, the correlation length actually depicts a pronounced peak and not a true divergence.

In Fig. 5(a) the correlation length is depicted as a function of τ on the logarithmic scale, assuming fixed parameters $V/U = 0.1$, $t/U = 0.303$, and $\mu/U = 0.18$. The solid curve represents $\tau > 0$ ($T > T_p$) whereas the dashed curve denotes $\tau < 0$ ($T < T_p$). The straight dashed-dot line reports the asymptotic limit $\xi \propto |\tau|^{-1}$ where we observe clearly the critical exponent $\nu = 1$ in the pseudo-critical regime. Note that when T is very close to T_p the power-law critical exponent fails, evidencing the ultimate nonsingular behavior of the thermodynamic quantities. A similar plot is depicted in Fig. 5(b), assuming the same set of parameters but for chemical potential $\mu/U = 1.28$. Here again we observe manifestly the critical exponents $\nu = 1$. Note that the power-law behavior holds for nearly two decades.

In order to have a clear picture of the range of temperatures around T_p on which the pseudo-critical regime holds, we can estimate crossover boundaries between the nonsingular and power-law regimes as well as between the power-law regimes and the low and high temperature ones. The nonsingular regime in the close vicinity of T_p emerges as the perturbation analysis fails. In the vicinity of the $\text{FRU}_2 - \text{AFM}_2$ ground-state transition, crossover lines can be built using $8w_{0,1}^2 = (w_{0,0} - 2w_{1,1})^2$, which separates the perturbative from the nonperturbative regimes. A similar crossover line can be written in the vicinity of the $\text{FRU}_4 - \text{AFM}_4$ ground-state transition [$8w_{1,2}^2 = (w_{2,2} - 2w_{1,1})^2$]. The power-law regime holds whereas the correlation length remains much larger than the lattice spacing. We will consider that crossover lines from the power law to the low and high temperature regimes satisfies $\xi = 10$. Equations (34) and (35) can be used to draw the respective crossover lines.

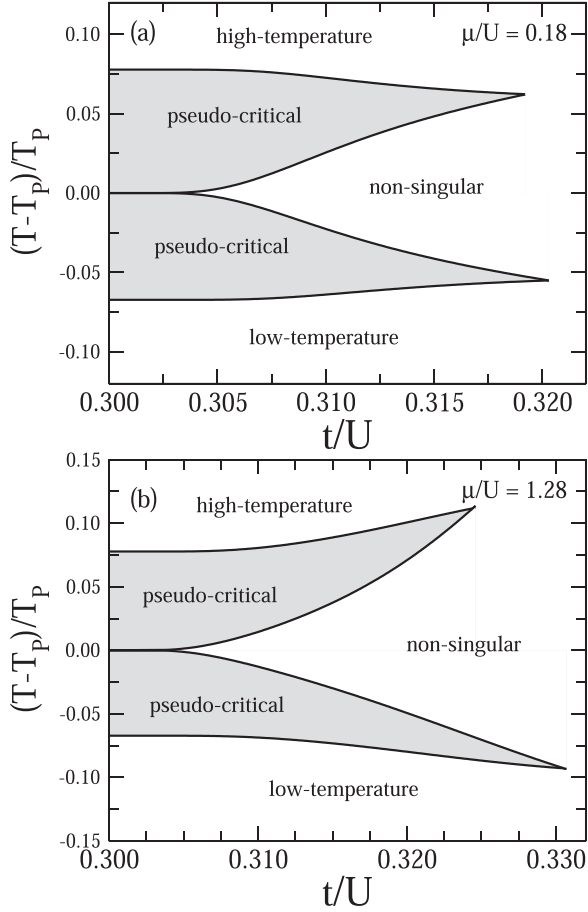


FIG. 5. Correlation length as a function of τ for fixed parameters $V/U = 0.1$, $t/U = 0.303$. The red line corresponds for $\tau > 0$ ($T > T_p$), and the dashed blue line denotes $\tau < 0$ ($T < T_p$), whereas the straight dashed-dot line reports $\xi \propto |\tau|^{-1}$. (a) For $\mu/U = 0.18$. (b) For $\mu/U = 1.28$.

In Fig. 6 we show the above crossover lines as a function the hopping parameter t in the close vicinities of the $\text{FRU}_2 - \text{AFM}_2$ and $\text{FRU}_4 - \text{AFM}_4$ boundary lines for an illustrative set of the other Hamiltonian parameters. First note that the width of the nonsingular regime decreases quite fast as one approaches $t_c = (U - V)/3$. Although the pseudo-transition temperature T_p decreases linearly, the nonsingular temperature range decays much faster.

One can determine how the range of the nonsingular regime decreases as t approaches t_c by recalling that only specific Boltzmann factors contribute to $w_{0,0}$, $w_{1,1}$, and $w_{0,1}$. The difference $|w_{0,0} - 2w_{1,1}|$ vanishes at T_p . Up to first order, it grows linearly with $|\Delta T|/T_p = |T - T_p|/T_p$ with the dominant contribution being

$$|w_{0,0} - 2w_{1,1}| \propto (|\Delta T|/T_p) e^{-E_{\text{AFM}_2}/k_B T_p}. \quad (43)$$

$w_{0,1}$ does not have contributions coming from neither of the ground states. At low temperatures, the dominant contribution for $w_{0,1}$ comes from the closest excited state giving $w_{0,1} = e^{-E_e/k_B T}$ with E_e being the energy of the lowest excited state. Therefore, for temperatures close to T_p , the crossover line between the nonsingular and the pseudo-critical regimes will satisfy $|\Delta T|/T_p \propto e^{-(E_e - E_{\text{AFM}_2})/k_B T_p}$. Recalling that $T_p \propto$

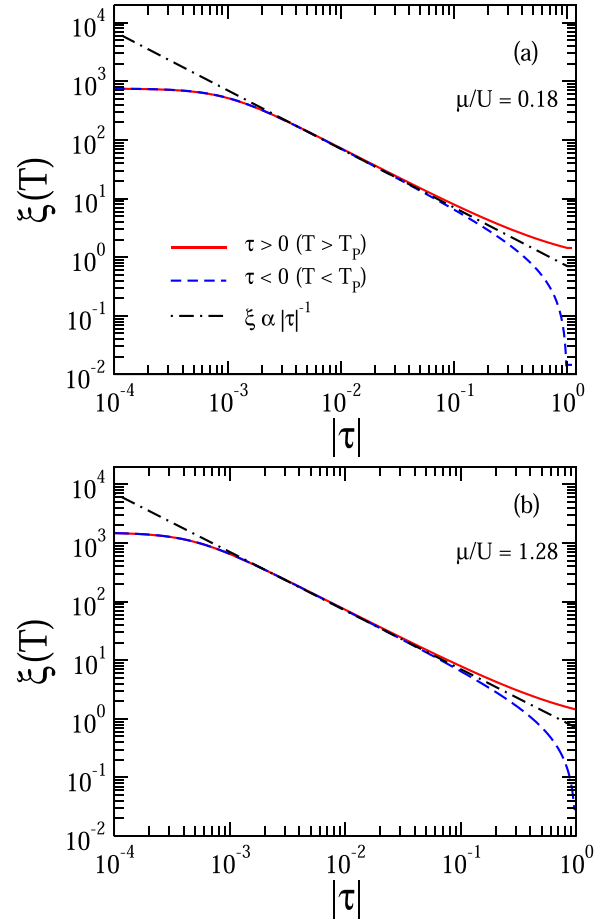


FIG. 6. Distinct temperature regimes as a function of the hopping parameter t in the close vicinity of the (a) $\text{FRU}_2 - \text{AFM}_2$ and (b) $\text{FRU}_4 - \text{AFM}_4$ ground-state transitions. Here we used $V/U = 0.1$, (a) $\mu/U = 0.18$, and (b) $\mu/U = 1.28$. The nonsingular regime becomes exponentially narrow as $t \rightarrow t_c = (U - V)/3 = 0.3U$ [see Eq. (44)]. The power-law regime holds for $\tau = (T - T_p)/T_p$ on the order of a few percent in the close vicinity of t_c . It dies away far from t_c when the perturbation and large correlation length conditions become incompatible.

($t - t_c$), the width of the nonsingular regime is found to decay as

$$|\Delta T|/T_p \propto e^{-a/(t-t_c)}, \quad (44)$$

with a being a constant at t_c that depends of the energy gap between the ground state and the first excited state with the nodal sites having distinct occupation numbers. The above asymptotic relation for the size of the nonsingular regime agrees with the numerical data.

The nonsingular regime widens as one departs from t_c . On the other hand, the crossover lines to the high and low temperature regimes are weakly dependent on t . Therefore, in the close vicinity of t_c , the power-law regime extends over a temperature range on the order of a few percent of T_p . The crossover lines delimiting the nonsingular and the high and low temperature regimes eventually meet. After this point, no preasymptotic power-law regime can be identified.

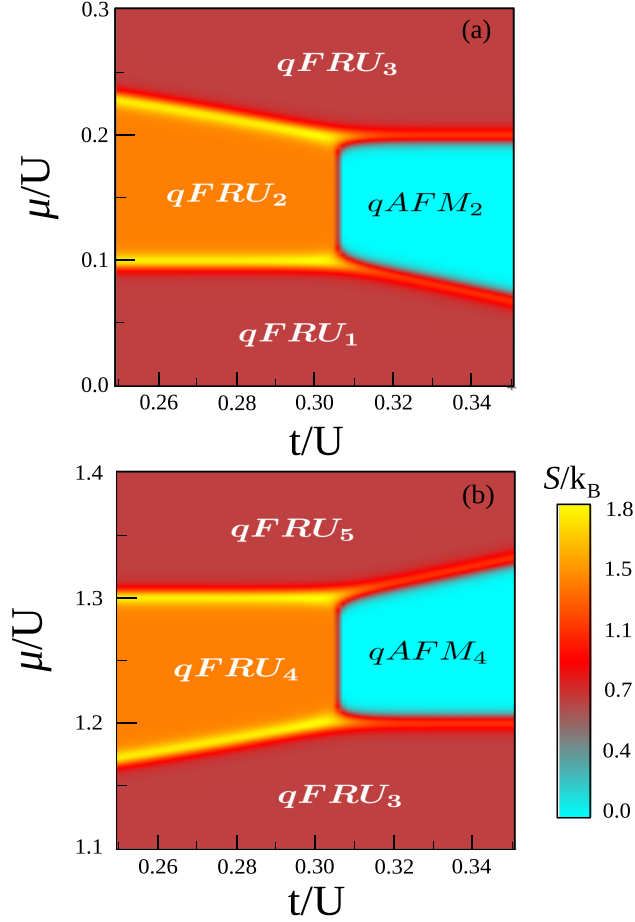


FIG. 7. Density plot of entropy on the plane t - μ , assuming fixed $V/U = 0.1$ and $k_B T/U = 0.005$. (a) For $\mu/U = [0, 0.3]$. (b) For $\mu/U = [1.1, 1.4]$.

IV. FIRST-ORDER-LIKE PSEUDO-TRANSITION

It is interesting to analyze some physical quantities, which are obtained as a first derivative of the free energy and exhibit an almost steplike behavior.

A. Entropy

In Fig. 7(a) we illustrate the density plot of entropy ($S = -\frac{\partial f}{\partial T}$) on the plane t - μ for fixed parameters $V = 0.1$ and $k_B T/U = 0.005$ for $\mu/U = [0, 0.3]$. This plot is depicted on the same scale of the phase diagram illustrated in Fig. 2(a). We definitely observe a pseudo-transition in the boundary of quasiantiferromagnetic ($qAFM_2$) and quasifrustrated ($qFRU_2$) phases characterized by a sharp boundary, whereas electron density remains constant $\rho = 2/3$. The regions are mostly governed by the zero temperature phases but due to thermal fluctuations the zero temperature phases become quasilong ranged because of the lack of actual spontaneous long-range order at any finite temperature. A similar density plot is illustrated in Fig. 7(b), assuming the same parameters but in the interval of $\mu/U = [1.1, 1.4]$. We can observe a steep entropy change in the boundary between the $qAFM_4$ and $qFRU_4$ phases where the electron density $\rho = 4/3$ per cell remains unaltered.

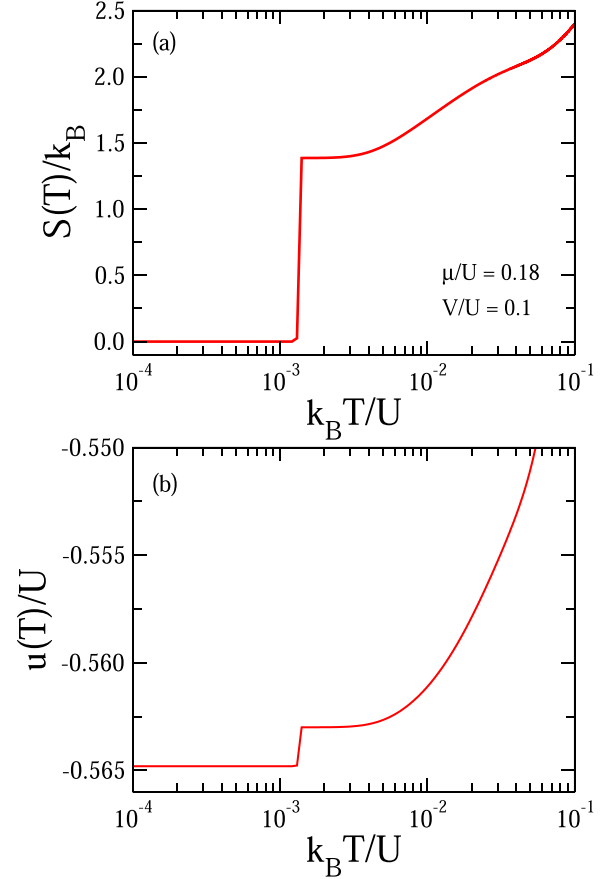


FIG. 8. (a) Entropy as a function of temperature on the semilogarithmic scale for fixed $t/U = 0.303$, $\mu/U = 0.18$, and $V/U = 0.1$. (b) Internal energy as a function of temperature on the semilogarithmic scale for fixed $t/U = 0.303$, $\mu/U = 0.12$, and $V/U = 0.1$.

In Fig. 8(a) we report the magnitude of entropy as a function of temperature on the semilogarithmic scale, assuming fixed parameters $t/U = 0.303$, $\mu/U = 0.18$, $V/U = 0.1$. Clearly one can observe a near step behavior at $k_B T_p/U \simeq 1.3 \times 10^{-3}$. For temperatures below T_p the entropy is almost null, which corresponds to the quasiantiferromagnetic phase ($qAFM_2$). On the other hand, the entropy has a plateau region ($qFRU_2$) with $S_0 = k_B \ln(4)$ for $T > T_p$. As the temperature is further increased, the entropy behaves, such as in standard models. Therefore, we observe a strong continuous change in entropy around the pseudo-transition, which typically resembles a discontinuous (first-order) phase-transition. However, we stress that it remains analytical at T_p .

B. Internal energy

The other quantity we discuss here is the internal energy $u(T) = TS + f$, which can also be obtained after a first derivative of the free energy.

In Fig. 8(b), the internal energy as a function of temperature in semilogarithmic scale is depicted for fixed $t/U = 0.303$, $\mu/U = 0.18$, and $V/U = 0.1$. Internal energy is continuous as a function of temperature, although it also shows a steep variation around the pseudo-critical temperature T_p . For temperatures below T_p , the internal energy leads to

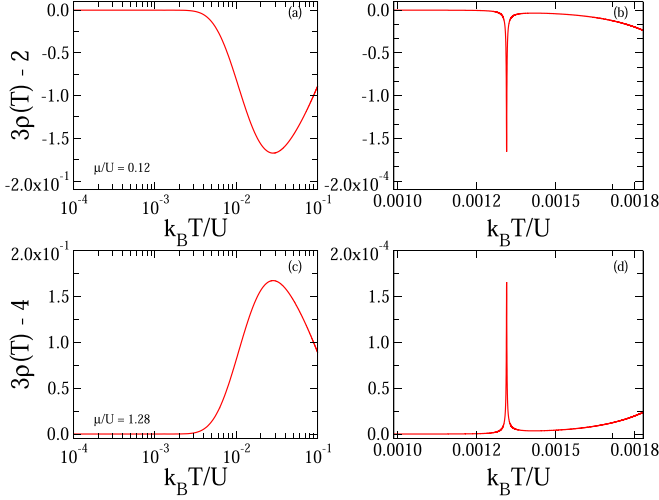


FIG. 9. Electron density as a function of temperature on the semilogarithmic scale for fixed $t/U = 0.303$ and $V/U = 0.1$. (a) For $\mu/U = 0.12$. (b) Zooming panel (a) around T_p . (c) For $\mu/U = 1.28$. (d) Zooming panel (c) around T_p .

$u/U = -0.5648$, which corresponds to the AFM_2 ground-state energy E_{AFM_2} . For $T > T_p$, the internal energy is mostly dominated by the FRU_2 ground-state energy $E_{\text{FRU}_2}/U = -0.563$.

C. The electron density

Another important quantity we explore is the thermal average electron density $\rho = -(\frac{\partial f}{\partial \mu})$ per unit cell.

In Fig. 9 the electron density as function of temperature is reported on the semilogarithmic scale for fixed $t/U = 0.303$, $V/U = 0.1$, and $\mu/U = 0.12$. At low temperatures, the electron density remains almost constant $\rho = 2/3$, up to roughly around $k_B T/U \sim 0.01$, and then the electron density decreases to $3\rho \approx 1.80$, and for higher temperature the electron density increases with temperature (for further details see Ref. [20]). Therefore, apparently no pseudo-critical behavior at T_p is evidenced in ρ . In Fig. 9(b) we plot the electron density as a function of temperature around pseudo-critical temperature. We observe a tiny depression at T_p reminiscent of the pseudo-transition due to thermal excitations to states with a single electron per unit cell (see the phase diagram).

Similarly, the electron density is depicted in Fig. 9(c) as function of temperature on the semilogarithmic scale, assuming same set of parameters, but for $\mu/U = 1.28$. Once again electron density remains almost constant $\rho = 4/3$ for temperatures below $k_B T/U \sim 0.01$, whereas for higher temperatures there is a peak reaching $\rho \approx 4.20$. In Fig. 9(d) we present a zooming plot of panel (c) around the pseudo-critical temperature where a tiny peak reminiscent of the pseudo-critical temperature is also present, reflecting thermal excitations to states with five electrons per unit cell (see the phase diagram). Surely we cannot expect any strong change in the electron density around T_p because the two competing ground states have equivalent electron densities.

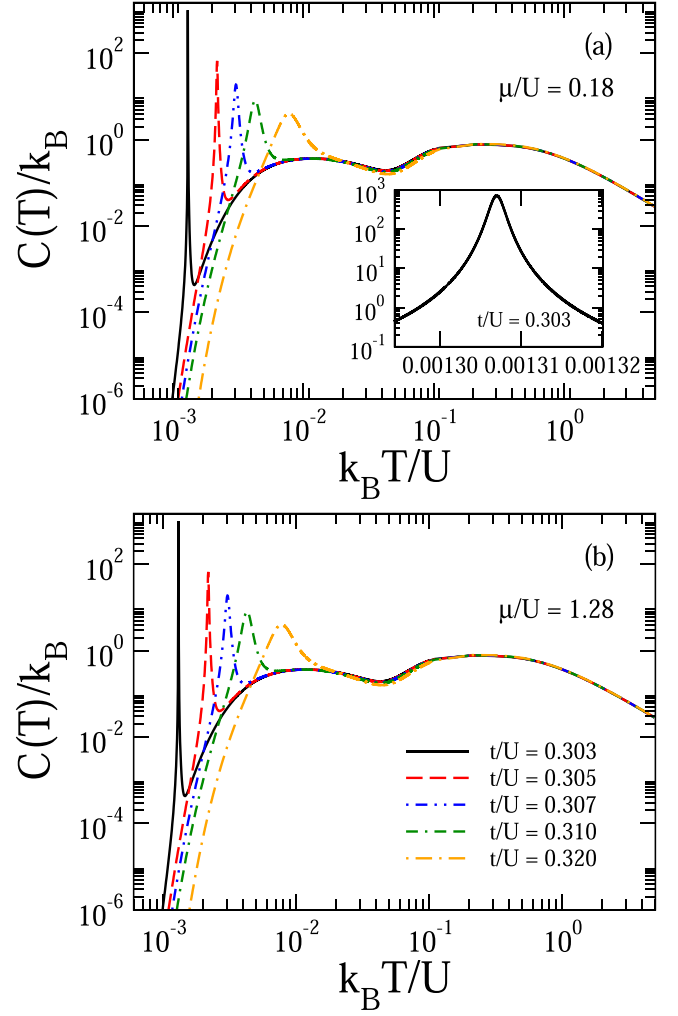


FIG. 10. Specific heat as a function of temperature on the logarithmic scale for $V/U = 0.1$. (a) For several values of t and $\mu/U = 0.18$ (in the vicinity of the $\text{FRU}_2 - \text{AFM}_2$ phase boundary). The inset: zooming around T_p . (b) For several values of t and $\mu/U = 1.28$ (in the vicinity of the $\text{FRU}_4 - \text{AFM}_4$ phase boundary).

V. SECOND-ORDER-LIKE PSEUDO-TRANSITION

Now let us turn our attention to the second-order derivative of the free energy. The following quantities exhibit trends quite similar to second-order phase-transition. It is important to reinforce that there is no singularity at T_p but just a rather sharp peak.

A. The specific heat

In Fig. 10, we display the specific heat $C = T(\frac{\partial S}{\partial T})$ as a function of temperature on the logarithmic scale assuming fixed $V/U = 0.1$. In panel (a) we depict for several values of t and $\mu/U = 0.18$ (close to the $\text{FRU}_2 - \text{AFM}_2$ ground-state transition). Here we see how the height of the peak increases, and the peak becomes sharper when $t/U \rightarrow 0.3$, whereas for t larger the height of the peak becomes lower and broader. At low temperatures, we observe clearly a huge sharp peak quite similar to a second-order phase-transition divergence around T_p . However, a zooming look as provided in the inner

plot around T_p evidences the rounded nature of the peak at the pseudo-critical temperature. Panel (b) reports the specific heat for the same set of parameters used in panel (a) but for $\mu/U = 1.28$ (close to the $\text{FRU}_4 - \text{AFM}_4$ ground-state phase-transition).

Now let us analyze the nature of the peak around T_p , looking for some critical exponent universality. For this purpose, we consider the specific heat around pseudo-critical temperature in the asymptotic limit (but not very close to T_p), which can be expressed according the discussion in Ref. [9] as

$$C(\tau) = T \left(\frac{\partial \mathcal{S}}{\partial \tau} \right) \left(\frac{\partial \tau}{\partial T} \right) \Big|_{T_p} = 2c_f \tau^{-3}, \quad (45)$$

where the coefficient c_f is given by

$$c_f = \begin{cases} \tilde{w}_{0,1}^2 c_{0,\xi}, & w_{0,0} \sim 2w_{1,1}, \\ \tilde{w}_{1,2}^2 c_{2,\xi}, & w_{2,2} \sim 2w_{1,1}. \end{cases} \quad (46)$$

Note that these preasymptotic coefficients also remain finite at T_p according to the same reasoning previously discussed for the correlation length coefficients, a feature also numerically confirmed. Therefore, the specific heat has the following preasymptotic expression when approaching the pseudo-critical temperature,

$$C(\tau) \propto |\tau|^{-\alpha}, \quad (47)$$

with pseudo-critical exponent $\alpha = 3$. The Hubbard diamond chain in the atomic limit also satisfies the pseudo-critical exponent found in Ref. [9]. However, it is worth stressing that this preasymptotic regime is only valid around the ascending and descending parts of the peak and surely fails very close to the peak top where the perturbation condition cannot prevail.

In order to confirm the above result. We report in Fig. 11(a) the $C(\tau)$ as a function of τ , assuming fixed parameters $V/U = 0.1$, $t/U = 0.303$, and $\mu/U = 0.18$ (near the $\text{FRU}_2 - \text{AFM}_2$ phase boundary). The continuous line represents data above T_p , whereas the dashed line corresponds data below T_p . The dashed-dot line describes the asymptotic function with critical exponent $\alpha = 3$. The straight line with angular coefficient $\alpha = 3$ fits accurately data over nearly two decades. Very close to T_p the power-law behavior breaks down, reflecting the actual analytic behavior of the specific heat. In panel (b) we plot the specific heat for $\mu/U = 1.28$ (near the $\text{FRU}_4 - \text{AFM}_4$ phase boundary), showing similar trends.

B. Compressibility

Another interesting quantity to be discussed is the isothermal electron compressibility [43] $\kappa_T = \frac{1}{\rho^2} \left(\frac{\partial \rho}{\partial \mu} \right)_T$ as a function of Hamiltonian parameters, temperature, and electron density.

In Fig. 12(a) the isothermal compressibility is shown as a function of temperature on the semilogarithmic scale, we observe a tiny peak at the pseudo-critical temperature. Magnifying around the pseudo-critical temperature [see Fig. 12(b)] it illustrated a double peak with local minimum at T_p . Since the pseudo-transition results from competing ground states with the same electron density, we actually cannot expect any giant peak of the electron compressibility at T_p because that would result in a pronounced electron density change.

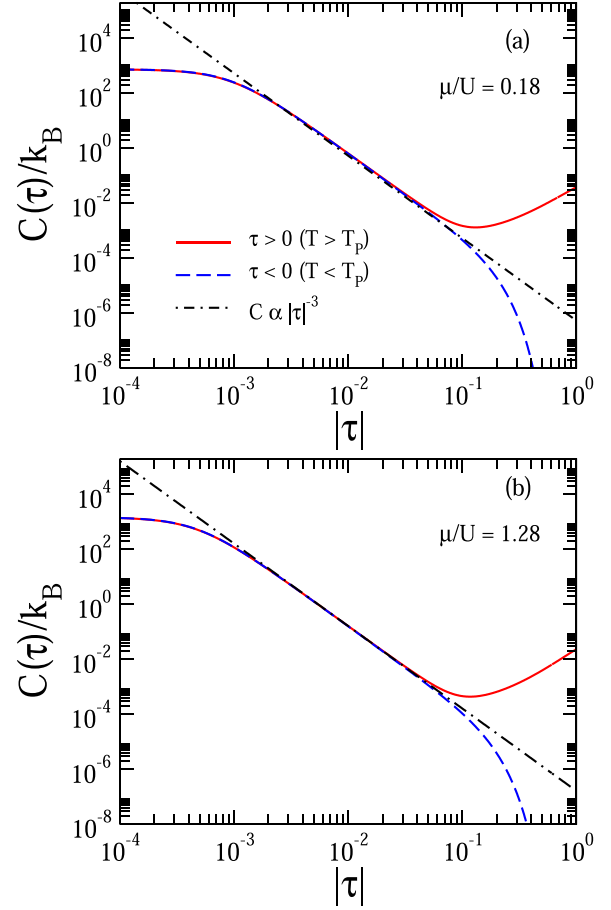


FIG. 11. Logarithmic specific heat as a function of $\ln(|\tau|)$ for fixed parameters $V/U = 0.1$, $t/U = 0.303$. The solid line corresponds for $\tau > 0$ ($T > T_p$), and the dashed line denotes $\tau < 0$ ($T < T_p$). The straight dashed-dot line reports $\xi \propto |\tau|^{-3}$. (a) For $\mu/U = 0.18$. (b) For $\mu/U = 1.28$.

VI. SUMMARY AND CONCLUSIONS

To summarize, we considered the extended Hubbard diamond chain restricted to the atomic limit with an arbitrary number of particles driven by chemical potential. The interaction between the dimer diamond chain and the nodal couplings are taken in the atomic limit (no hopping), whereas dimer interaction includes the hopping term. We showed that this model exhibits a pseudo-transition effect in the low temperature region. The internal energy and entropy were shown to change quite abruptly in a very narrow range of temperatures around the pseudo-transition when the physical parameters are properly tuned in a close vicinity of special ground-state phase-transitions. The correlation length and specific heat display pronounced peaks with well defined power laws in a well defined temperature range in the vicinity of the pseudo-transition point. The pseudo-critical exponents associated with the correlation length and specific heat were shown to be $\nu = 1$ and $\alpha = 3$, respectively. These are the same pseudo-exponents reported to hold in spin models with Ising-like interactions, pointing towards a universal behavior of pseudo-transitions [9,10]. We also demonstrated that the electron density and respective electronic compressibility

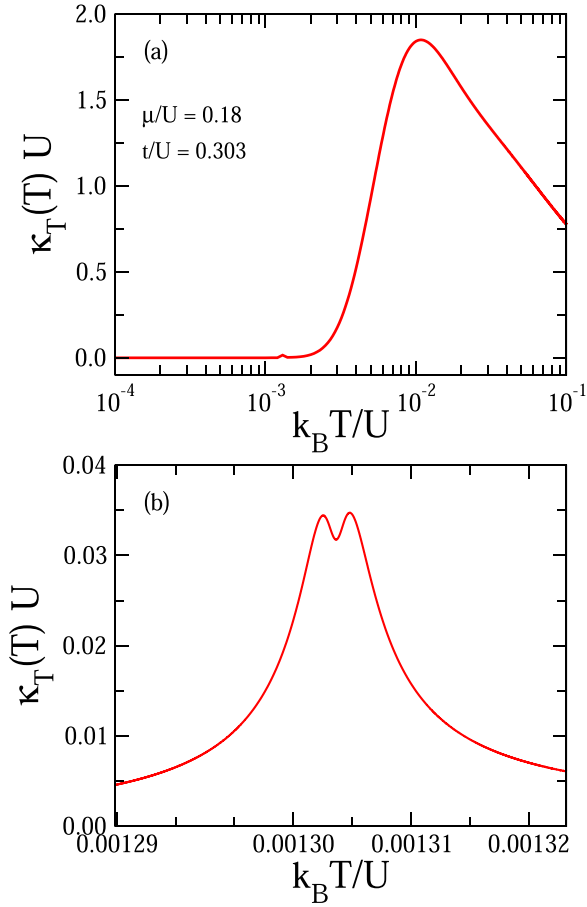


FIG. 12. Isothermal compressibility as a function of temperature on the semilogarithmic scale for fixed $t/U = 0.303$, $\mu/U = 0.18$, and $V/U = 0.1$. (b) Magnified around T_p .

displays reminiscent signatures of the pseudo-transition. The present results add to the general understanding of the remarkable phenomenon of pseudo-transitions taking place at finite temperatures in one-dimensional equilibrium systems having structured interactions within the relevant unit cell.

ACKNOWLEDGMENTS

This work was supported by Coordenação de Aperfeiçoamento de Pessoal de Nível Superior (CAPES), Conselho Nacional de Desenvolvimento Científico e Tecnológico (CNPq), Fundação de Apoio à Pesquisa do Estado de Alagoas (FAPEAL), and Fundação de Apoio à Pesquisa do Estado de Minas Gerais (FAPEMIG). J.T. thanks Brazilian agency CNPq Grant No. 159792/2019-3 for full partial support.

APPENDIX A: REAL ROOTS OF THE CUBIC EQUATION

The transfer matrix is a symmetric matrix, so its eigenvalues are guaranteed to be real values. Therefore, here we verify the cubic equation (23) roots must be different and real numbers, given by (25).

Obviously, we can convince that both Q and R are real numbers from (27) and (28).

Now let us verify the real number Q is positively defined by using the cubic equation coefficients (25), thus, after some algebraic manipulation we obtain the following expression:

$$Q = \frac{1}{9}(w_{2,2} - \frac{1}{2}w_{0,0} - w_{1,1})^2 + \frac{1}{12}(w_{0,0} - 2w_{1,1})^2 + \frac{2}{3}w_{0,1}^2 + \frac{1}{3}w_{0,2}^2 + \frac{2}{3}w_{1,2}^2, \quad (\text{A1})$$

which is strictly a positive number ($Q > 0$) since all Boltzmann factors are positive. According to a cubic equation property, this condition is enough to conclude that three the eigenvalues of transfer matrix will be different and real numbers.

Now the question is to determine which are the largest and the lowest eigenvalues? Since all eigenvalues must be real and different because $Q > 0$. Which implies that the solution (25) must satisfy the following restriction $\phi \neq \pm n\pi$ with $n = \{0-2, \dots\}$. Therefore, we can choose ϕ conveniently such that $0 < \phi < \pi$. Thus, we have the following trigonometric relation,

$$\cos\left(\frac{\phi}{3}\right) > \cos\left(\frac{\phi - 2\pi}{3}\right) > \cos\left(\frac{\phi - 4\pi}{3}\right), \quad (\text{A2})$$

if we multiply all terms of inequalities by $2\sqrt{Q} > 0$ and adding $-\frac{a_3}{3}$ to all expressions (note that $a_3 < 0$), thus, we conclude that

$$\Lambda_0 > \Lambda_1 > \Lambda_2. \quad (\text{A3})$$

Note that if $\phi = 0$, in principle, we would have $\Lambda_1 = \Lambda_2$ but this condition is forbidden because $Q > 0$. Similar for $\phi = \pi$ we have $\Lambda_0 = \Lambda_1$, but again this condition cannot be satisfied since $Q > 0$. Therefore, we have identified which eigenvalues is the largest one and the lowest one.

Of course we can choose other intervals equivalently and verify how the eigenvalues are ordered. In Table II the eigenvalues for each interval is reported. The open intervals of ϕ guarantees all eigenvalues must be real and different values in order to satisfy the condition $Q > 0$.

The three cubic root solutions are exchanging periodically which depends on the interval of ϕ , making a bit puzzle to identify which eigenvalue is the largest one. In Table II it is reported how the eigenvalues are ordered. In each interval the solutions are equivalent because other intervals simply exchange the eigenvalues with no relevance. Therefore, here we conveniently choose the first interval $\phi \in (0, \pi)$, so the eigenvalues must be ordered as following $\Lambda_0 > \Lambda_1 > \Lambda_2$.

Even more, according to the Perron-Frobenius theorem, the largest eigenvalue must be nondegenerate and positive.

APPENDIX B: PERTURBATIVE TRANSFER MATRIX CORRECTION

In order to study the pseudo-transition property in the low temperature region, we need to analyze the transfer matrix in the low temperature region. In principle, the cubic root solution could be a bit cumbersome task to identify as an easy handling solutions. A simple strategy to obtain a reasonable solution could be considering the transfer matrix (19) as a sum

of two matrices $\mathbf{V} = \mathbf{V}_0 + \zeta \mathbf{V}_1$. The first term is given by

$$\mathbf{V}_0 = \begin{bmatrix} w_{0,0} & 0 & w_{0,2} \\ 0 & 2w_{1,1} & 0 \\ w_{0,2} & 0 & w_{2,2} \end{bmatrix}, \quad (\text{B1})$$

This matrix can be considered as the unperturbed transfer matrix, whose eigenvalues are

$$u_0^{(0)} = \frac{1}{2}[w_{0,0} + w_{2,2} + s], \quad (\text{B2})$$

$$u_1^{(0)} = 2w_{1,1}, \quad (\text{B3})$$

vskip3pt

$$u_2^{(0)} = \frac{1}{2}[w_{0,0} + w_{2,2} - s], \quad (\text{B4})$$

where $s = \sqrt{d^2 + 4w_{0,2}^2}$ and $d = w_{0,0} - w_{2,2}$.

In the limit of $w_{0,2} \rightarrow 0$, the unperturbed solution can eventually satisfy the following relation:

$$u_0^{(0)} = u_1^{(0)}. \quad (\text{B5})$$

This condition leads to a pseudo-transition, which we can simplify

$$w_{0,0} = 2w_{1,1} \quad \text{for } w_{0,0} > w_{2,2}, \quad (\text{B6})$$

$$w_{2,2} = 2w_{1,1} \quad \text{for } w_{0,0} < w_{2,2}. \quad (\text{B7})$$

The above condition is essential to find pseudo-critical temperature T_p .

The second term of the transfer matrix is given by

$$\mathbf{V}_1 = \begin{bmatrix} 0 & \sqrt{2}w_{0,1} & 0 \\ \sqrt{2}w_{0,1} & 0 & \sqrt{2}w_{1,2} \\ 0 & \sqrt{2}w_{1,2} & 0 \end{bmatrix}. \quad (\text{B8})$$

Close to the pseudo-critical temperature, the elements of matrix \mathbf{V}_1 become smaller than the elements of matrix \mathbf{V}_0 . Therefore, we can find the transfer matrix eigenvalues by using a perturbative approach.

Consequently, the solution of the transfer matrix after a standard perturbative manipulation up to the first-order term gives us the following root corrections:

$$u_0^{(1)} = \frac{[(s-d)w_{1,2} + 2w_{0,2}w_{0,1}]^2}{s(s-d)(u_0^{(0)} - 2w_{1,1})}, \quad (\text{B9})$$

$$u_1^{(1)} = -u_0^{(1)} - u_2^{(1)}, \quad (\text{B10})$$

$$u_2^{(1)} = \frac{[(s+d)w_{1,2} - 2w_{0,2}w_{0,1}]^2}{s(s+d)(u_2^{(0)} - 2w_{1,1})}. \quad (\text{B11})$$

As a consequence of the perturbative correction, the transfer matrix eigenvalues becomes

$$\Lambda_j = u_j^{(0)} + \zeta u_j^{(1)} + O(\zeta^2), \quad j = \{0, 1, 2\}. \quad (\text{B12})$$

Assuming the elements of matrix \mathbf{V}_1 are small, we can obtain an approximate result of (25), fixing $\zeta = 1$. Hence, it is evident that the largest eigenvalue of the transfer matrix will be Λ_0 , even when $u_0^{(0)} = u_1^{(0)}$ since $u_0^{(1)} > 0$ and $u_1^{(1)} < 0$.

-
- [1] S. M. de Souza and O. Rojas, *Solid State Commun.* **269**, 131 (2018).
 - [2] I. M. Carvalho, J. Torrico, S. M. de Souza, O. Rojas, and O. Derzhko, *Ann. Phys. (NY)* **402**, 45 (2019).
 - [3] J. Torrico, M. Rojas, S. M. de Souza, O. Rojas, and N. S. Ananikian, *Eur. Phys. Lett.* **108**, 50007 (2014).
 - [4] J. Torrico, M. Rojas, S. M. de Souza, and O. Rojas, *Phys. Lett. A* **380**, 3655 (2016).
 - [5] J. Strečka, *Acta Phys. Pol., A* **137**, 610 (2020).
 - [6] L. Galisova and J. Strecka, *Phys. Rev. E* **91**, 022134 (2015).
 - [7] O. Rojas, J. Strečka, and S. M. de Souza, *Solid State Commun.* **246**, 68 (2016).
 - [8] J. Strecka, R. C. Alecio, M. L. Lyra, and O. Rojas, *J. Magn. Magn. Mater.* **409**, 124 (2016).
 - [9] O. Rojas, J. Strecka, M. L. Lyra, and S. M. de Souza, *Phys. Rev. E* **99**, 042117 (2019).
 - [10] T. Hutak, T. Krokhamalskii, O. Rojas, S. M. de Souza, and O. Derzhko, *Phys. Lett. A* **387**, 127020 (2021).
 - [11] I. Daruka and Z. Gulacsi, *Phys. Rev. E* **58**, 5403 (1998).
 - [12] I. S. Hagemann, Q. Huang, X. P. A. Gao, A. P. Ramirez, and R. J. Cava, *Phys. Rev. Lett.* **86**, 894 (2001).
 - [13] J. van Lierop and D. H. Ryan, *Phys. Rev. Lett.* **86**, 4390 (2001).
 - [14] O. Derzhko, A. Honecker, and J. Richter, *Phys. Rev. B* **79**, 054403 (2009).
 - [15] O. Derzhko, J. Richter, A. Honecker, M. Maksymenko, and R. Moessner, *Phys. Rev. B* **81**, 014421 (2010).
 - [16] O. Derzhko and J. Richter, *Phys. Rev. B* **90**, 045152 (2014).
 - [17] R. R. Montenegro-Filho and M. D. Coutinho-Filho, *Phys. Rev. B* **74**, 125117 (2006).
 - [18] R. R. Montenegro-Filho, F. S. Matias, and M. D. Coutinho-Filho, *Phys. Rev. B* **102**, 035137 (2020).
 - [19] Z. Gulacsi, A. Kampf, and D. Vollhardt, *Phys. Rev. Lett.* **99**, 026404 (2007); *Suppl. Prog. Theor. Phys.* **176**, 1 (2008).
 - [20] O. Rojas, S. M. de Souza, and N. S. Ananikian, *Phys. Rev. E* **85**, 061123 (2012).
 - [21] O. Krupnitska, *Phys. Rev. B* **102**, 064403 (2020).
 - [22] J. Torrico, M. Rojas, M. S. S. Pereira, J. Strečka, and M. L. Lyra, *Phys. Rev. B* **93**, 014428 (2016).
 - [23] B. Nachtergaele, J. P. Solovej, and J. Yngvason, *Condensed Matter Physics and Exactly Soluble Models*, Selecta of E. H. Lieb (Springer, Berlin-Heidelberg, 2004).
 - [24] G. Beni and P. Pincus, *Phys. Rev. B* **9**, 2963 (1974).
 - [25] F. Mancini, *Eur. Phys. J. B* **47**, 527 (2005).
 - [26] F. Mancini and F. P. Mancini, *Phys. Rev. E* **77**, 061120 (2008).
 - [27] O. Rojas and S. M. de Souza, *Phys. Lett. A* **375**, 1295 (2011).
 - [28] A. A. Lopes and R. G. Dias, *Phys. Rev. B* **84**, 085124 (2011).
 - [29] B. M. Lisnii, *Low Temp. Phys.* **37**, 296 (2011).
 - [30] K. C. Rule, A. U. B. Wolter, S. Sullow, D. A. Tennant, A. Bruhl, S. Kohler, B. Wolf, M. Lang, and J. Schreuer, *Phys. Rev. Lett.* **100**, 117202 (2008).
 - [31] H. Kikuchi, Y. Fujii, M. Chiba, S. Mitsudo, T. Idehara, T. Tonegawa, K. Okamoto, T. Sakai, T. Kuwai, and H. Ohta, *Phys. Rev. Lett.* **94**, 227201 (2005); H. Kikuchi, Y. Fujii, M. Chiba, S. Mitsudo, T. Idehara, T. Tonegawa, K. Okamoto, T. Sakai, T. Kuwai, K. Kindo, A. Matsuo, W. Higemoto, K. Nishiyama,

- M. Horvatić, and C. Bertheir, *Prog. Theor. Phys. Suppl.* **159**, 1 (2005).
- [32] L. Canova, J. Strecka, and M. Jascur, *J. Phys.: Condens. Matter* **18**, 4967 (2006).
- [33] N. S. Ananikian, L. N. Ananikyan, L. A. Chakhmakchyan, and O. Rojas, *J. Phys.: Condens. Matter* **24**, 256001 (2012).
- [34] L. Chakhmakchyan, N. Ananikian, L. Ananikyan, and C. Burdik, *J. Phys.: Conf. Ser.* **343**, 012022 (2012).
- [35] S.-S. Deng, S.-J. Gu, and H.-Q. Lin, *Phys. Rev. B* **74**, 045103 (2006).
- [36] M. S. S. Pereira, F. A. B. F. de Moura, and M. L. Lyra, *Phys. Rev. B* **77**, 024402 (2008); **79**, 054427 (2009).
- [37] H. Jeschke, I. Opahle, H. Kandpal, R. Valenti, H. Das, T. Saha-Dasgupta, O. Janson, H. Rosner, A. Bruhl, B. Wolf, M. Lang, J. Richter, S. Hu, X. Wang, R. Peters, T. Pruschke, and A. Honecker, *Phys. Rev. Lett.* **106**, 217201 (2011).
- [38] B. Gu and G. Su, *Phys. Rev. B* **75**, 174437 (2007); O. Derzhko and J. Richter, *Eur. Phys. J. B* **52**, 23 (2006).
- [39] J. Vidal, B. Doucot, R. Mosseri, and P. Butaud, *Phys. Rev. Lett.* **85**, 3906 (2000).
- [40] B. Doucot and J. Vidal, *Phys. Rev. Lett.* **88**, 227005 (2002).
- [41] M. Cui, N. Wang, S. Zhang, and Z. He, *Cryst. Growth Des.* **19**, 547 (2019).
- [42] O. Rojas, *Chin. J. Phys.* **70**, 157 (2021).
- [43] R. J. Baxter, *Exactly Solved Models in Statistical Mechanics*, (Academic, New York, 1982).
- [44] Y. Saito, *Prog. Theor. Phys.* **59**, 375 (1978).